Journal of Molecular Modeling (2021) 27: 241
https://doi.org/10.1007/s00894-021-04862-6

ORIGINAL PAPER

Electronic, optical, and vibrational properties of $B_3N_3H_6$ from first-principles calculations

Yun-Dan Gan[1] · Han Qin[2] · Fu-Sheng Liu[3] · Zheng-Tang Liu[4] · Cheng-Lu Jiang[3] · Qi-Jun Liu[3]

Received: 27 April 2021 / Accepted: 29 July 2021 / Published online: 8 August 2021

Abstract

The structural, electronic, optical, and vibrational properties of $B_3N_3H_6$ have been calculated by means of the first-principles density functional theory (DFT) calculations within the generalized gradient approximation (GGA) and the local density approximation (LDA). The calculated structural parameters of $B_3N_3H_6$ are in good agreement with experimental data. The obtained band structure of $B_3N_3H_6$ shows that it has an indirect band gap with 5.007 eV, indicating that it presents insulation characteristic. The total and partial density of states (DOS) of $B_3N_3H_6$ are given, which tell us the states of the orbital occupation. With the band structure and density of states, we have analyzed the optical properties including the complex dielectric function, refractive index, absorption, conductivity, loss function, and reflectivity. By the contrast, it is found that optical anisotropy is observed in the (001) direction and (100) direction. Moreover, the vibrational properties have been obtained and analyzed, showing that $B_3N_3H_6$ is dynamically stable due to that there is no imaginary frequency. The frequencies associating with the vibrations are given, which show that $B_3N_3H_6$ has a low mechanical modulus and thermal conductivity.

Keywords Density functional theory · Electronic structure · Optical properties · $B_3N_3H_6$

Introduction

Borazine ($B_3N_3H_6$), which is generally introduced in textbooks as "inorganic benzene" under aspects of the isoelectronic relationship [1], is an ideal precursor for boron nitride materials because it only contains elements of boron, nitrogen, and hydrogen [2]. It has been used as the precursor for preparation of both boron nitride ceramic matrix composites by precursor infiltration pyrolysis (PIP) and boron nitride coatings by chemical vapor deposition (CVD) [3]. Borazine was originally discovered by the thermal decomposition of the diammoniate of diborane [4]. Both experimental [5, 6] and theoretical [7, 8] works have been performed widely. The thermal decomposition of $B_3N_3H_6$ in unsaturated vapor has been studied [9], showing that the gaseous $B_3N_3H_6$ was decomposed on the reaction vessel surface along with the formation of volatile intermediates. The nature of chemical bond [10], ring current strengths [11], and anion-π interactions [12] of $B_3N_3H_6$ were investigated, indicating its wide applications such as active molecule for electrodes [13], reactant for boron nitride nanowalls [14], low-dimensional spin filters [15, 16]. etc.

Kalemos [10] compared the nature of the chemical bond in $B_3N_3H_6$, $B_3O_3H_3$, $B_2N_2C_2H_6$, and related species by considering the excited states of the constituent fragments, which told us that these molecules isoelectronic to benzene were formed due to that BH, CH, NH binded together in their excited states. Rabanal-León et al. [11] investigated the ring current strengths of $B_3N_3X_6$ (X = H, F, Cl, Br, I, At) by using the magnetically induced current density method, which were used to evaluate the corresponding contributions to aromaticity. Bauzá et al. [12] studied the rings of N_6, $B_3O_3H_3$, $B_3N_3H_6$, B_3N_3, and $B_3S_3H_3$ with the anion-π interactions, which were important to crystal

✉ Cheng-Lu Jiang
juul@my.swjtu.edu.cn

✉ Qi-Jun Liu
qijunliu@home.swjtu.edu.cn

1 Xi'an Modern Chemistry Research Institute, Xi'an 710065, People's Republic of China

2 School of Science, Xihua University, Chengdu 610039, People's Republic of China

3 School of Physical Science and Technology, Southwest Jiaotong University, Chengdu 610031, People's Republic of China

4 State Key Laboratory of Solidification Processing, Northwestern Polytechnical University, Xi'an 710072, People's Republic of China

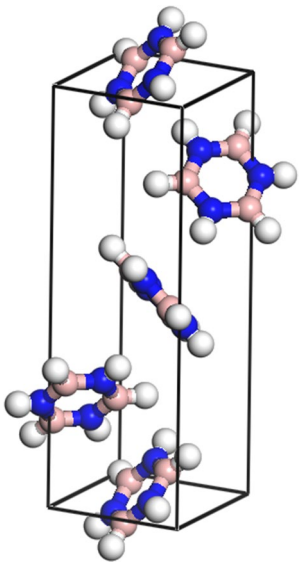

Fig. 1 The crystal structure of $B_3N_3H_6$ (B atoms are pink, N atoms are blue, and H atoms are white)

packing and three-dimensional structure. Sen [13] used $B_3N_3H_6$ as active molecule to investigate the role of asymmetric magnetic electrodes. Merenkov et al. [14] synthesized hexagonal boron nitride nanowalls from $B_3N_3H_6$ and NH_3 gas mixture.

However, there are few studies in the literatures about physical properties of $B_3N_3H_6$. For example, the optical and vibrational properties associated with the material's structure are important to the military and civilian applications [17, 18], which have not been reported systematically. The optical properties of the material are critical to the application of laser guidance, optical information processing, telecommunications, infrared countermeasures, radar detection, etc. [19–21]. The vibrational properties are linked with the chemical reaction process, molecular bonding strength, Raman spectra, etc. [22–24], which are very important to understand the explosion process of energetic materials. Therefore, our purpose is to calculate the electronic structure, optical, and vibrational properties of $B_3N_3H_6$ by using the first-principles density functional theory.

Computational details

The first-principles calculation with the Cambridge Sequential Total Energy Package (CASTEP) is employed in this paper [25]. The LDA of Ceperley-Alder-Perdew-Zunger (CAPZ) functional as well as GGA of

Table 1 The optimized structural parameters of $B_3N_3H_6$ along with the results of previous experimental data

	This work			Experimental data [1]
	LDA	GGA PBE-G	GGA PBE-TS	
a (Å)	4.787	5.115	5.315	5.463
c (Å)	13.699	15.264	16.204	16.315

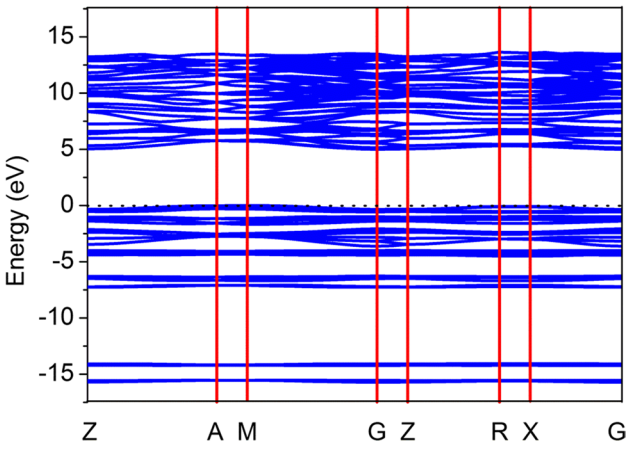

Fig. 2 The band structure of $B_3N_3H_6$ from the GGA PBE-TS calculation

Perdew-Burke-Ernzerhof (PBE) functional are applied as the exchange–correlation functional [26–29]. In order to consider the van der Waals interactions in $B_3N_3H_6$ crystal, the DFT-TS [30] and DFT-D2 [31] methods are used. The pseudopotential is an effective potential constructed to replace the ionic core states, that is, the valence electrons are

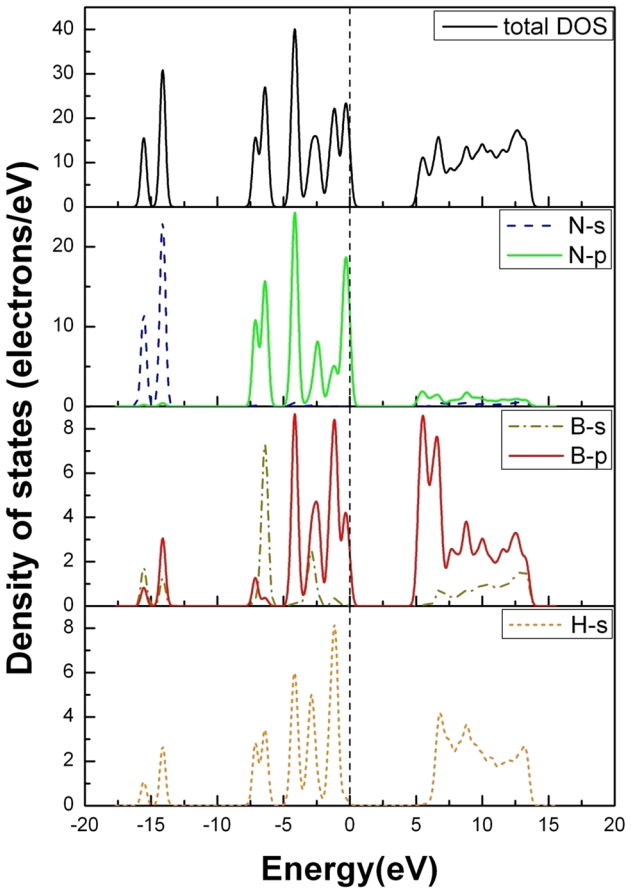

Fig. 3 The density of states of $B_3N_3H_6$ from the GGA PBE-TS calculation

described by pseudo-wave functions [26–29]. For $B_3N_3H_6$, the ionic cores are represented by ultrasoft pseudopotential. For B atom, the configuration is $1s^2 2s^2 2p^1$, where the $2s^2$ and $2p^1$ electrons are treated as valence electrons; for N atom, the configuration is $1s^2 2s^2 2p^3$, where the $2s^2$ and $2p^3$ electrons are treated as valence electrons; for H atom, the configuration is $1s^1$, where the $1s^1$ electron is treated as valence electron. The energy cutoff of 500 eV is applied in plane-wave basis. The Brillouin-zone integration is performed with $3 \times 3 \times 1$ meshes using the Monkhorst–Pack method [32] for structure optimization. The values of the convergence thresholds for total energy, maximum force, maximum stress, and maximum displacement are 5.0×10^{-6} eV/atom, 0.01 eV/Å, 0.02 GPa, and 5.0×10^{-4} Å.

Results and discussion

Structural properties

The space group of tetragonal structure $B_3N_3H_6$ is $P4_32_12$. The crystal mode of $B_3N_3H_6$ is shown in Fig. 1 after structural optimization, and it is an equilibrium crystal structure of Borazine. The optimized structural parameters of $B_3N_3H_6$ are given in Table 1 as well as experimental data [1]. It can be seen that the values based on the GGA PBE-TS functional are in good agreement with the experimental results, indicating that this functional can well describe the crystal structure of Borazine. Hence, the physical properties of Borazine are solved by the GGA PBE-TS in the following work.

Electronic properties

The calculated band structure of $B_3N_3H_6$ within the GGA PBE-TS is shown in Fig. 2. From the band structure, it is shown that $B_3N_3H_6$ has an indirect band gap because the top of valence band is found at G point, while the bottom of conduction band is found at A point. The band gap is calculated to be 5.007 eV, so we can know that $B_3N_3H_6$ is an insulator. The calculated band gap value is smaller than the experimental value of 6.5 eV [33]. The discrepancy is due to the well-known underestimation of DFT calculations. In order to solve this discrepancy, we use the B3LYP hybrid functional to recalculate the band structure. The

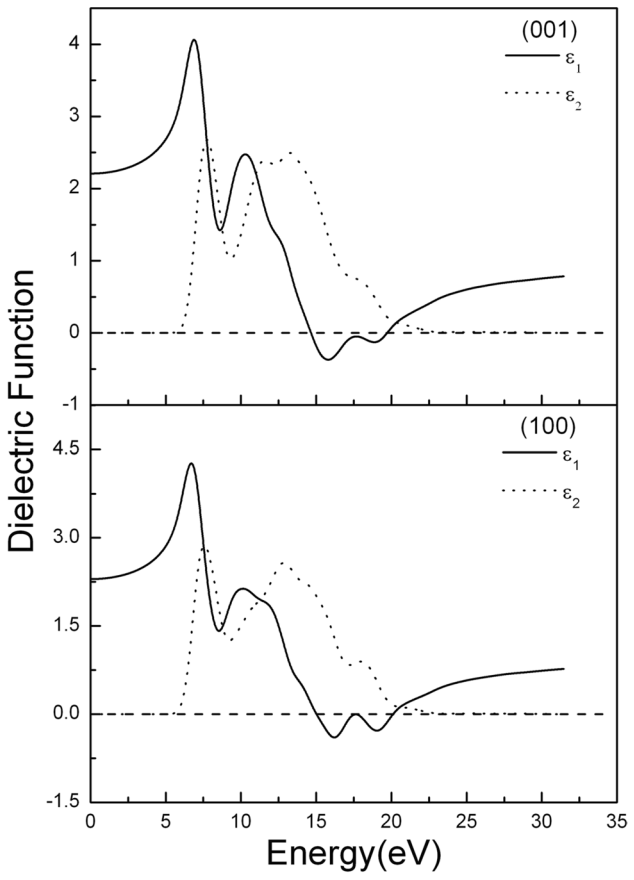

Fig. 4 The real and imaginary part of dielectric function of $B_3N_3H_6$ for polarization direction (001) and (100)

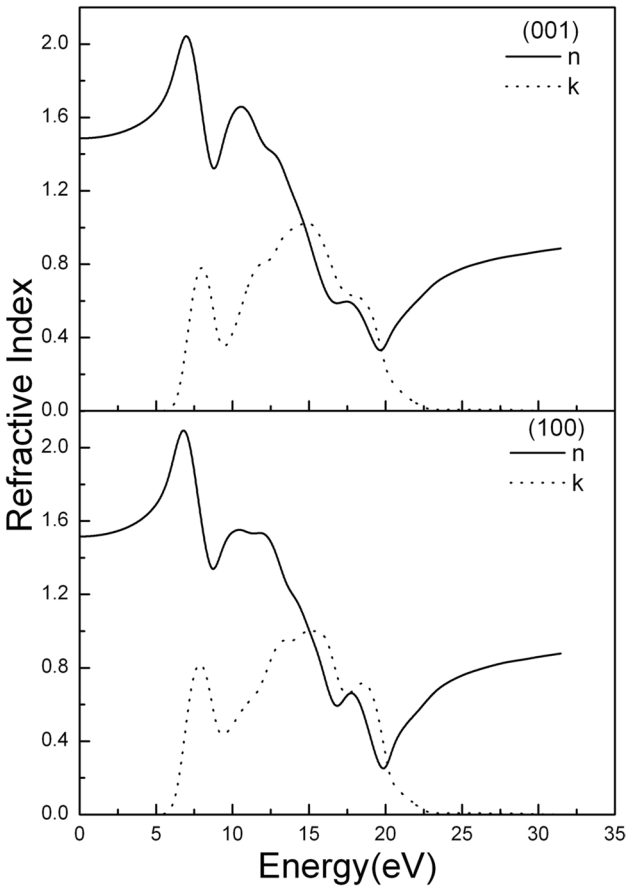

Fig. 5 The real and imaginary part of refractive index of $B_3N_3H_6$ for polarization direction (001) and (100)

calculated bandgap is 6.711 eV which is close to experimental value.

In the band structure, the valence bands are roughly divided into three regions: − 16.0 eV to − 14.0 eV (lower), − 7.5 eV to 6.0 eV (middle), and − 4.5 eV to 0 eV (higher). Figure 3 shows the total and the partial density of states (DOS) of $B_3N_3H_6$. With the states between − 16 eV and − 12.5 eV, there is the interaction of N 2 s, B 2p and H 1 s. The states between – 8 eV and – 5 eV are predominantly composed of N 2p, B 2 s and all hydrogen's 1 s. The valence bands basically arise from interaction of N 2p, B 2p and H 1 s states in the Fermi level.

Optical properties

The optical properties such as the complex dielectric function, complex refractive index, complex conductivity function, reflectivity, loss function, and absorption coefficient are important, which can be obtained from the complex dielectric function [34]:

$$\varepsilon(\omega) = \varepsilon_1(\omega) + i\varepsilon_2(\omega) \quad (1)$$

In this section, we present our results of optical properties of $B_3N_3H_6$ at the equilibrium lattice constants in Figs. 4–9, up to an energy of 35 eV. We resolve the optical properties into two independent components: the polarization direction (001) component and the polarization direction (100) component. The calculated real part and imaginary part of complex dielectric function of $B_3N_3H_6$ are shown in Fig. 4. From this figure, the real part of complex dielectric function is $\varepsilon_{1\,(001)} = 2.209$ and $\varepsilon_{1\,(100)} = 2.298$. There is a peak ($\omega_{(001)} = 7.735$ eV, $\omega_{(100)} = 7.577$ eV) from 4.5 eV to 9 eV for imaginary part, which is attributed to transition from the valence bands to conduction bands (t_{2g}). There is a peak ($\omega_{(001)} = 13.225$ eV, $\omega_{(100)} = 12.863$ eV) for the calculated imaginary part, which is due to transition from the valence bands to conduction bands (e_g). The complex refractive index of $B_3N_3H_6$ is shown in Fig. 5. As shown in Fig. 5, we find that the static refractive index is $n_{(001)}(0) = 1.486$ and $n_{(100)}(0) = 1.516$. The refractive index reaches a peak at energy of 6.979 eV in (001) component, while it reaches a peak at energy

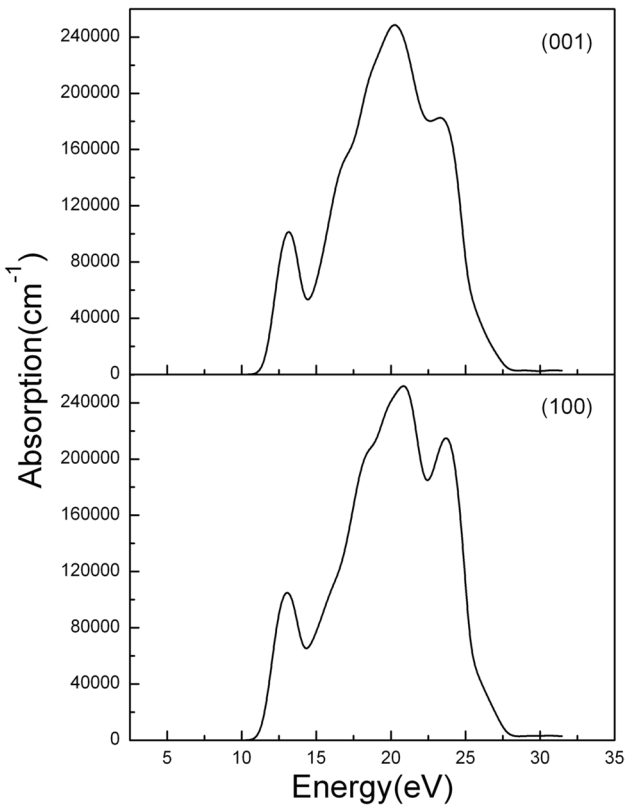

Fig. 6 The absorption coefficient of $B_3N_3H_6$ for polarization direction (001) and (100)

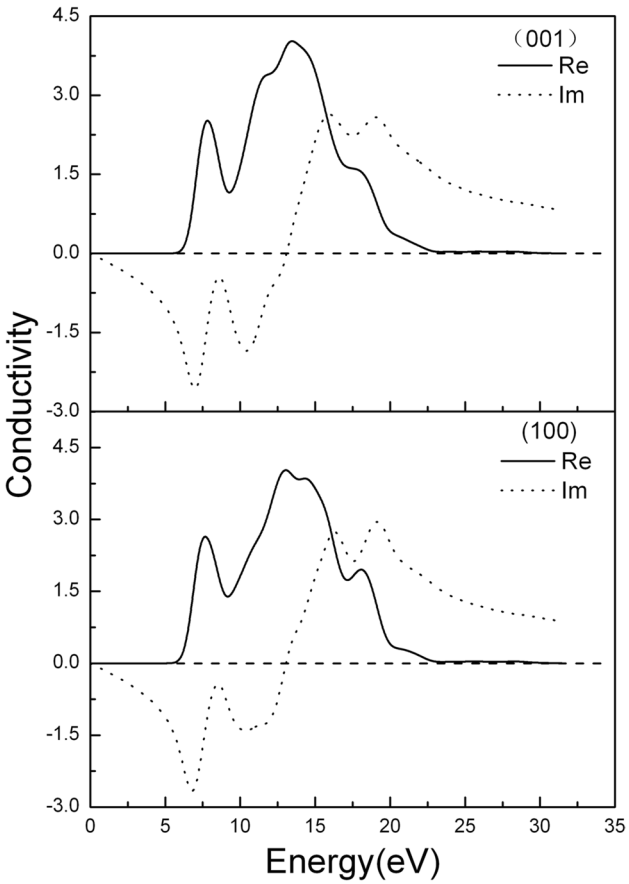

Fig. 7 The complex conductivity of $B_3N_3H_6$ for polarization direction (001) and (100)

of 6.806 eV in (100) component. Figures 6, 7, 8 and 9 show the absorption coefficient α(ω), complex conductivity function σ(ω), energy-loss function L(ω), and optical reflectivity R(ω). In each figure, as we can see, the optical anisotropy corresponds to the space group of $B_3N_3H_6$.

Vibrational properties

As shown in Fig. 10, there are 144 vibrations including 3 acoustic branches and 141 optical branches. The phonon spectra with no imaginary frequency reveal that $B_3N_3H_6$ is dynamically stable. There is no significant splitting, which indicates that the $B_3N_3H_6$ has no ability to change the strength of light as an optical device.

As shown in Fig. 10, the frequencies around 3450 cm^{-1} are referred to the vibrations of B-H and N–H, which are parallel to plane (111) , (111) , (111) and (111), including anti-symmetry and symmetry vibrations. It indicates that the B-H and N–H have a most dynamic strength. The frequencies around 2550 cm^{-1} are B-N anti-symmetric and symmetric vibrations, which are also parallel to above four

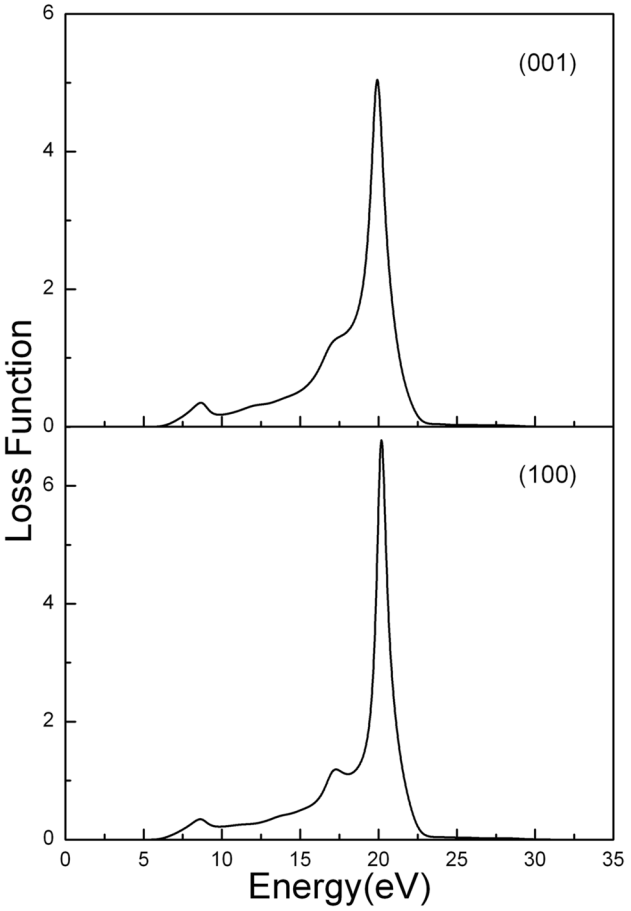

Fig. 8 The energy-loss function of $B_3N_3H_6$ for polarization direction (001) and (100)

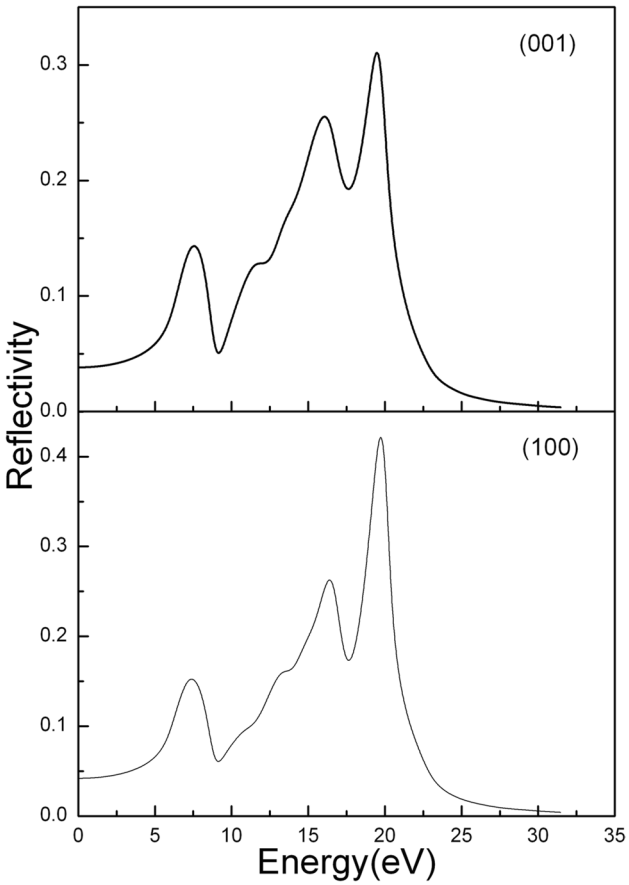

Fig. 9 The optical reflectivity of $B_3N_3H_6$ for polarization direction (001) and (100)

planes. According to the calculated results, the vibrations of the frequencies above 896 cm^{-1} are parallel to four planes. The vibration of phonon is parallel to four planes at high frequencies; it shows that the crystal has a better dynamic stable when the optical radiation along those planes. Below 890 cm^{-1}, the vibrations begin to be perpendicular and

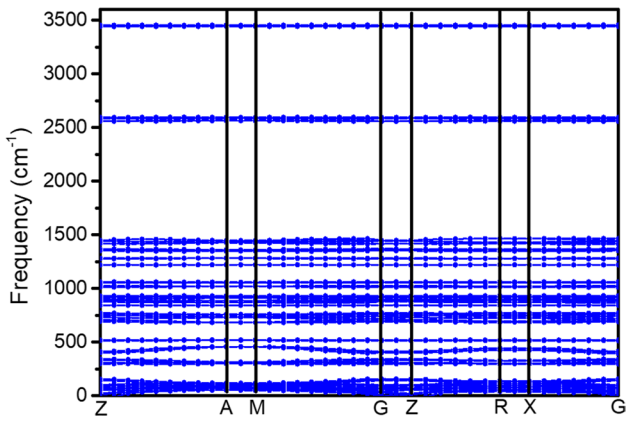

Fig. 10 Calculated phonon dispersion of $B_3N_3H_6$

parallel to four planes as well as group vibration. It corresponds to a weak covalent bond strength, so the crystal has a low mechanical modulus and thermal conductivity. In a word, these vibrations can be used to present conformational changes and bonding and to reflect the initiation mechanism of energetic materials [24].

Conclusions

We have investigated the structural, electronic, optical, and vibrational properties of $B_3N_3H_6$. We find that the accurate equilibrium volume of $B_3N_3H_6$ from DFT calculations can be obtained by the TS correction to treat the van der Waals interactions. From the calculated band structure and density of states, we conclude that $B_3N_3H_6$ is an insulator with an indirect band gap of 5.007 eV. The obtained optical properties show an optical anisotropy in (100) and (001) due to its tetragonal structure. These peaks associated with the transitions from the occupied to unoccupied states in the imaginary part of dielectric function are given. Moreover, the vibrational properties of $B_3N_3H_6$ have been computed and these vibrations are discussed, indicating that $B_3N_3H_6$ shows weak covalent bond strength.

Author contribution Yun-Dan Gan: writing — original draft, investigation, methodology, data curation. Han Qin: methodology, conceptualization. Fu-Sheng Liu: theoretical analysis, formal analysis. Zheng-Tang Liu: visualization, software. Cheng-Lu Jiang: formal analysis, validation, writing — review and editing. Qi-Jun Liu: conceptualization; writing, review and editing; supervision.

Availability of data and materials The datasets supporting the results of this work are included within the article; the other datasets generated during the current study are available from the corresponding author on reasonable request.

Code availability Not applicable.

Declarations

Conflict of interest The authors declare no competing interests.

References

1. Boese R, Maulitz AH, Stellberg P (1994) Chem Ber 127:1887
2. Lei MK, Ma TC (1996) J Inorg Mater 11:329
3. Li JS, Zhang CR, Li B (2011) Bulletin of the Chinese Ceramic Society 30:567
4. Wideman T, Sneddon LG (1995) Inorg Chem 34:1002
5. Chiavarino B, Crestoni ME, Marzio AD, Fornarini S, Rosi M (1999) J Am Chem Soc 121:11204
6. Islas R, Chamorro E, Robles J, Heine T, Santos JC, Merino G (2007) Struct Chem 18:833
7. Peyerimhoff SD, Buenker RJ (1970) Theoret Chim Acta 19:1
8. Kiran B, Phukan AK, Jemmis ED (2001) Inorg Chem 40:3615
9. Zavgorodnii AS, Timoshkin AYu (2018) Russian J General Chem 88:2476
10. Kalemos A (2018) Int J Quantum Chem. 118:e25650
11. Rabanal-León WA, Tiznado W, Alvarez-Thon L (2019) Int J Quantum Chem 119:e25859
12. Bauzá A, Quiñonero D, Deyà PM, Frontera A (2012) Chem Phys Lett 530:145
13. Sen S (2017) Chem Phys 491:126
14. Merenkov IS, Kosinova ML, Maximovskii EA (2017) Nanotechnology 28:185602
15. Zhang CX, Guo H, Yang Z, Luo YH (2012) Acta Phys. Sin. 61:193601
16. Shao P, Ding LP, Luo DB, Lu C (2020) Molecular Phys. 118:e1667542
17. Mammeri F, Bourhis EL, Rozes L, Sanchez C (2005) J Mater Chem 15:3787
18. Qin H, Zeng W, Liu FS, Gan YD, Tang B, Zhu SH, Liu QJ (2021) J Energ Mater 39:125
19. Wang Y, Luo MJ, Zhao P, Che XL, Cao YZ, Huang FQ (2020) CrystEngComm 22:3526
20. Jia N, Xiong XX, Wang SP, Yu TT, Han B, Qiao J, Li CN, Tao XT (2018) CrystEngComm 20:7802
21. Zhang X, Zhao HL, Gao S, Zeng QF (2021) J Rare Earths 39:453
22. Wu XW, Liu ZC, Ji GF, Zhu WH (2019) J Molecular Graphics Modelling 90:144
23. Huang W, He ZY, Zhao BJ, Zhu SF, Chen BJ (2019) J Alloys Compounds 796:138
24. Su Y, Fan JY, Zheng ZY, Zhao JJ (2018) Comput Mater Sci 153:392
25. Clark SJ, Segall MD, Pickard CJ, Hasnip PJ, Probert MIJ, Refson K, Payne MC (2005) Z Kristallogr 220:567
26. Ceperley DM, Alder BJ (1980) Phys Rev Lett 45:566
27. Perdew JP, Zunger A (1981) Phys Rev B 23:5048
28. Perdew JP, Burke K, Ernzerhof M (1996) Phys Rev Lett 77:3865
29. Perdew JP, Chevary JA, Vosko SH, Jackson KA, Pederson MR, Singh DJ, Fiolhais C (1992) Phys Rev B 46:6671
30. Tkatchenko A, Scheffler M (2009) Phys Rev Lett 102:073005
31. Grimme S (2006) J Comput Chem 27:1787
32. Monkhorst HJ, Pack JD (1976) Phys Rev B 13:5188
33. Zunger A (1974) J Phys C: Solid State Phys 7:76
34. Gao J, Zeng W, Tang B, Zhong M, Liu QJ (2021) Mater Sci Semicond Process 121:105447